

Interstitial Fe-Cr alloys: Tuning of magnetism by nanoscale structural control and by implantation of nonmagnetic atoms

Interstitial Fe-Cr alloys

N. Pavlenko¹, N. Shcherbovskikh², and Z.A. Duriagina²

¹ Institute for Condensed Matter Physics, National Academy of Sciences of Ukraine, Svientsitsky str.1, 79011 Lviv, Ukraine; e-mail: pavlenko@mailaps.org

² Institute for Applied Mathematics and Fundamental Sciences, Lviv Technical University, Ustyianowycha str. 10, 79013 Lviv, Ukraine

the date of receipt and acceptance should be inserted later

Abstract. Using the density functional theory, we perform a full atomic relaxation of the bulk ferrite with 12.5%-concentration of monoatomic interstitial Cr periodically located at the edges of the bcc Fe_α cell. We show that structural relaxation in such artificially engineered alloys leads to significant atomic displacements and results in the formation of novel highly stable configurations with parallel chains of octahedrally arranged Fe. The enhanced magnetic polarization in the low-symmetry metallic state of this type of alloys can be externally controlled by additional inclusion of nonmagnetic impurities like nitrogen. We discuss possible applications of generated interstitial alloys in spintronic devices and propose to consider them as a basis of novel durable types of stainless steels.

1 Introduction

Last years demonstrate increased activities in the search for novel materials exhibiting controlled modification of electronic properties by inclusion or implantation of different atoms or ionic groups. A prominent example of the implantation-altered systems is the stainless steel. In the steels, the implantation of chromium, molybdenum, nitrogen and other chemical elements substantially changes the microstructure of subsurface layers and modify their corrosion resistance and hardness [1].

In the development of novel efficient multifunctional materials for technological applications in the long-term devices, the properties like hardness, corrosion, heat resistance and other types of mechanical and chemical durability are of central interest [2,3]. It frequently appears in science and technology that well known materials doped by different chemical elements exhibit unexpected physical properties not revealed previously.

As an example of such a new unexpected behavior, in the present work we consider an alloy Fe-Cr. The alloys of Fe and Cr, doped by C, Ni and by other elements, are widely used as basic components for ferritic and martensitic steels. Substitutional alloys of Fe and Cr have attracted much attention of theory and experiment due to their rich magnetic properties characterized by local antiferromagnetism in the proximity of Cr atoms implanted into ferromagnetic iron [4,5,6,7]. Due to small differences between the atomic radii of iron and chromium, the modification of the substitutional alloy properties is limited

to the local magnetic transformation due to local changes in the electronic orbital occupancies, without significant structural modifications. In contrast to the substitutional structural configurations, the interstitial Fe-Cr alloys considered in the present work contain Cr impurities which are located in the interstitial positions of the bcc lattice of Fe_α. In the recent theoretical studies of the Cr interstitials in Fe-Cr alloys, different types of interstitial configurations were analyzed. Among them, a pair configuration $\langle 111 \rangle$ dumbbell is considered as the most energetically favourable which requires about 4.2eV for its formation under irradiation [8,9].

In the present work, we consider a novel monoatomic interstitial configuration which contains single Cr atoms positioned in the centers of the edges of the bcc ferrite. In contrast to the substitutional alloys, the significant forces due to the interstitial atoms induce substantial structural optimization which enhances the volume due to modified lattice constants and leads to the relaxation of the atomic positions in the unit cell. We find that the relaxation of the initial bcc unit cell results in significant atomic distortions and in the formation of atomic chain-like structures. As appears in the density-functional-theory (DFT) calculations of the optimized structures, the energy gain achieved due to the structural relaxation of the considered interstitial alloy can approach 6.17 eV which makes this type of systems highly stable and durable. In the present work, we propose to consider these artificially generated alloys as candidates for novel types of stainless steels.

The fundamental difference between the industrial alloys and the alloys studied in the present work is the ordered and periodic character of the latter. In the industrial steels, the amorphous character of the systems is related to the random distribution of the impurities. The hardening of the steels proceeds through the surface treatment and is accompanied by formation of granular microstructure with the spatially inhomogeneous impurity concentration and modified subsurface properties [11]. In the studies of the subsurface Cr-doped alloyed ferrite, we consider the supercells containing periodically located Cr atoms in the cubic lattice of Fe_α . The interstitial Cr induces significant atomic reconstruction with consequent break of initial cubic symmetry and stabilization of a new lower-symmetry state. The appearing structural transformation has a character of a phase transition which occurs due to nanoscale tailoring of cubic Fe by interstitial inclusion of Cr atoms, the effect which can be experimentally verified by the means of modern methods like AFM spectroscopy.

Using the DFT-based structural optimization, we obtain the optimized atomic microstructure of a chain-like character where the chains of octahedrally arranged Fe atoms are formed along the (001)-axis. We find that the competing ferromagnetic and antiferromagnetic interactions lead to spatially inhomogeneous spin polarization. The magnetization of the structurally relaxed system is significantly enhanced as compared to the pure ferrite without Cr inclusions. The obtained enhancement makes the generated alloys perspective candidates for spin polarizers in spintronic applications. In the generated chain-like structures, the relaxation is accompanied by the formation of spatial channels with extremely low carrier density. We suggest that these channels can be considered as paths for the low-barrier-migration of light impurities like H, N, Li or C. As an example of a light atom in the interstitial alloy, we study of the migration paths of nonmagnetic nitrogen and calculate the energy barriers along the migration paths. We obtain a strong influence of the nonmagnetic N on the alloy magnetization. Our findings show that the structural modifications due to possible nanoscale tuning of Cr impurities on the edges of bcc cubic cells of iron can play a central role in the control of their electronic properties.

2 Structural relaxation of interstitial alloy Fe_α -Cr

The present studies of the electronic properties of the considered interstitial Fe-Cr alloy are based on the DFT calculations of the electronic structure of the systems generated by periodic translation of specially chosen supercells. The initial supercell shown in Fig. 1 contains the doubled 2×2 cubic bcc cell of ferrite (Fe_α) and a single Cr atom centered in one of the edges of the Fe_α cubic unit cell with the lattice constant $a = 3.85 \text{ \AA}$. The obtained structure is described by a chemical formula Fe_8Cr and determines an interstitial Fe-Cr alloy with the Cr concentration $n = 0.125$ which is typical for stainless steels.

The presence of interstitial Cr leads to significant local forces acting on the neighbouring Fe atoms. To minimize the forces, the coordinates of all atoms have been relaxed. In the present studies, the optimization of the supercell has been performed by employing the DFT approach implemented with the linearized augmented plane wave (LAPW) scheme in the full potential Wien2k code [13]. To study the role of the spin polarization in the structural relaxation, two different relaxation procedures have been employed. In the first procedure, the atomic optimal positions are calculated in the local density approximation (LDA) on a $2 \times 2 \times 5$ k-points grid. To explore the role of spin degrees of freedom in the relaxation, in the second procedure the local spin density approximation (LSDA) has been used in the optimization of the structure. The results of both methods of the structural relaxation are presented in Fig. 2.

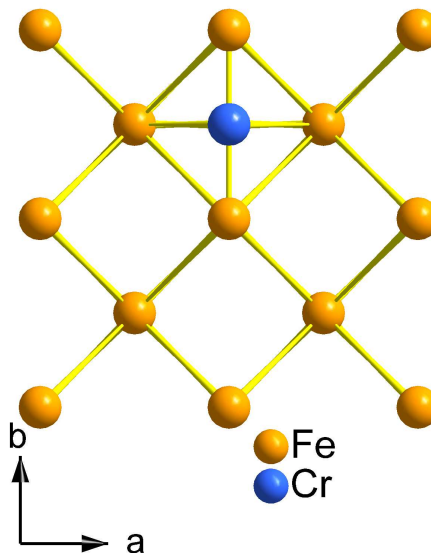


Fig. 1. Schematic view of unrelaxed 2×2 Fe_α cell which contain 12.5% of edge-centered interstitial Cr.

A central common feature which characterizes both (LDA- and LSDA-relaxed) structures is the clusterization of the sublattice of the iron atoms. In the LDA-optimized structure (Fig. 2(a)), the relaxation results in formation of a high-symmetry clusterized network. This network consists of the Fe_6 -octahedra which form the square plaquettes in the (x, y) ((a, b)) plane with Cr atoms located in the center of each plaquette. The distance from the centered Cr to each nearest iron octahedra amounts 1.9 \AA . Despite the significant displacements of the iron atoms from their initial positions, the net electric polarization of the cell is zero due to high structural symmetry $C4/m$ obtained after the relaxation.

The formation energy of the relaxed Fe_8Cr -configuration can be expressed as

$$E_f(\text{LDA}) = E_{\text{tot}}(\text{Fe}_8\text{Cr}) - 8E_{\text{tot}}(\text{Fe}) - E_{\text{tot}}(\text{Cr}),$$

where the last two terms identify the total energies of the bulk bcc Fe_α and Cr, respectively. To determine $E_{\text{tot}}(\text{Fe})$, we have calculated the total energy value of the bulk Fe_α in the ferromagnetic state. As the LSDA-calculation of the spin-polarized configurations of the bulk Cr are converged to the paramagnetic state, we consider the total energy $E_{\text{tot}}(\text{Cr})$ for the paramagnetic Cr. With these values, we find that $E_f(\text{LDA}) = 4.82\text{eV}$. To analyze the role of the relaxation, we have also calculated the energy $E_f(\text{unrel})$ of the formation of initial unrelaxed configuration which is equal to 5.02eV . As a consequence, the significant energy gain due to the structural relaxation

$$\Delta E(\text{LDA}) = E_f(\text{unrel}) - E_f(\text{LDA}) = 0.196\text{eV},$$

shows a central importance of the atomic displacements for the stability of the considered systems.

The optimization procedure based on the LSDA approach accounts for additional corrections due to spin polarization and produces new ordered structural patterns presented in Fig. 2(b) and Fig. 2(c) for two different (unrelaxed $a = b = 2.86\text{\AA}$ and relaxed $a = b = 3\text{\AA}$) lattice constants. The volume-optimized structure (c) is signified by the 13%th increase of the unit cell volume due to the insertion of the interstitial Cr. The LSDA-optimized structural pattern is characterized by the chains of atomic Fe-groups along the $x(a)$ -direction, each group containing six Fe-atoms. The nearest chains are separated by a distance about 4\AA and are connected to each other by the Fe-Cr bonds of the length about 2.4\AA for the structure (b) with $a = 2.86\text{\AA}$, and 2.7\AA for the structure (c) with the optimized $a = 3.0\text{\AA}$. The local antiferromagnetic ordering in the vicinity of Cr is characterized by the magnetic moments $\mu_{\text{Cr}} = -0.72 \mu_B$ and $\mu_5 = 2.4 \mu_B$ and $\mu_6 = 1.25 \mu_B$ of the neighbouring atoms Fe5 and Fe6, respectively. The magnetic moments of more distant iron atoms have the values around $2.5 \mu_B$, which is close to results obtained for substitutional alloys and in pure Fe_α [8].

As compared to the tetragonal structure of the LDA-optimized system, the chain-like structure of the LSDA-relaxed supercell is characterized by substantially lower crystal symmetry and by the absence of the inversion center. In contrast to the LDA-based configurations, the formation energy of the LSDA-relaxed Fe_8Cr configuration $E_f(\text{LSDA}) = E_{\text{tot}}(\text{Fe}_8\text{Cr}) - 8E_{\text{tot}}(\text{Fe}) - E_{\text{tot}}(\text{Cr}) = -1.15\text{eV}$ is negative which implies its high stability. We can also calculate the energy gain due to the structural relaxation by the LSDA approach

$$\Delta E(\text{LSDA}) = E_f(\text{unrel}) - E_f(\text{LSDA}) = 6.17\text{eV},$$

which also demonstrates the high stability of the relaxed spin-polarized structure and a necessity to account for a spin polarization in the structural optimization of the systems with strong magnetoelastic effect.

2.1 Magnetic properties

In the considered systems, we have also analyzed modification of the local magnetic properties due to the relaxation of the interatomic distances. To see how the atomic

displacements influence the spin polarization of the surrounding atoms, in Fig. 3 we present the dependences of the local moments of Cr and of two nearest neighboring Fe on the Cr displacement along the bond [Fe5-Cr-Fe6]

$$\Delta = [x(\text{Cr}) - x(\text{Fe5})] - [x(\text{Cr}) - x(\text{Fe5})]^0,$$

where $[x(\text{Cr}) - x(\text{Fe5})]^0$ is the optimized [Fe5-Cr]-bond length. The increase of Δ leads to the change of μ_{Cr} from $-0.7 \mu_B$ to the value about $-0.73 \mu_B$. In addition, the larger Δ implies the elongation of the [Fe5-Cr] bond and lead to the reduced $\mu_5 = 2.39 \mu_B$ due to the tendency for a suppression of antiferromagnetism in the vicinity of Fe5. The increase of Δ also produces an enhancement of μ_6 from $1.25 \mu_B$ to the values about $1.28 - 1.3 \mu_B$, an opposite trend which occurs due to the shortening of the bond between Cr and Fe6.

In Fig. 3, the Δ -dependences of the atomic magnetic moments are highly asymmetric with respect to Δ . Consequently, the obtained magnetoelastic coupling produces an anisotropy of the magnetic moments and is accompanied by the loss of the inversion center due to the atomic displacements, the effect which can be observed in Fig. 2(b) and (c). In Fig. 2(c), the low-symmetry structure corresponds to the minimum of the total energy. As a conclusion, the neglect of the magnetoelastic coupling in the electronic structure calculations does not allow to achieve a full optimization in this type of interstitial alloys.

2.2 Electronic structure

Fig. 4 shows the $3d$ spin-polarized electronic density contours of the LSDA-optimized structure in the (x, z) plane. One can see that the majority $3d$ spin-up states of Fe are highly occupied by the electrons whereas the electron concentration of Cr spin up states is substantially lower. In contrast to this, the spin-down (minority) electrons are characterized by high electron occupation of Cr and lower electron density on Fe. In Fig. 4, the chain-like structures Fe-Cr in the z -direction are characterized by strong hybridization between the intra-chain $3d$ spin-down orbitals of Fe and Cr. The last feature leads to the spatial charge redistribution and to higher charge densities on the bonds between spin-down Cr and Fe. In the LSDA-optimized system, the structural optimization produces areas with low charge density in the y (b)-direction, where each area can be identified between the chains of Fe-octahedra. As can be seen in Fig. 4, these areas are almost free of the charge and can be considered as channels for the migration of light atoms like H, Li or N. Similarly to the contours in Fig. 4, the electron density of the majority Fe and Cr orbitals and on the bonds between Cr and Fe calculated for the LDA-optimized structure (Fig. 5) is substantially lower than the charge density on the spin-down contours, although the spatial charge distribution is more homogeneous as compared to that in Fig. 4.

For the LDA-relaxed structure, the density of states is characterized by strong suppression of the majority spin-up DOS at the Fermi level (Fig. 6(a)), whereas the minority DOS at the Fermi level remains significant. Similar,

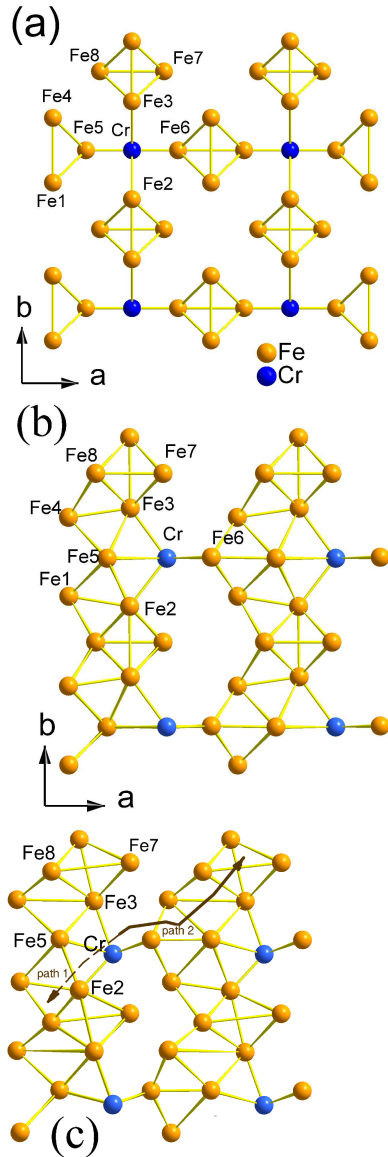


Fig. 2. Relaxed structure of Fe with 12.5% of Cr: (a) LDA calculations, (b) spin-polarized LSDA calculations in the structure with $a = b = 2.86$ Å and (c) spin-polarized LSDA calculations in the structure with $a = b = 3.0$ Å. The path 1 and path 2 identify possible paths for diffusion through the channels formed due to atomic relaxation.

although much stronger, suppression of majority DOS is typically observed in half-metallic systems where the electric current is conducted by the electrons with the same direction of spin [14]. In contrast to the half-metallic-like features of the LDA-relaxed structure, the DOS of the LSDA-optimized system (Fig. 6(b)) demonstrates substantial values at the Fermi level for both spin directions which implies an enhancement of the metallic state for the majority electrons.

In transition metal oxides, the metallic state obtained in the LDA approach is usually strongly influenced by additional account for the local Coulomb corrections for the

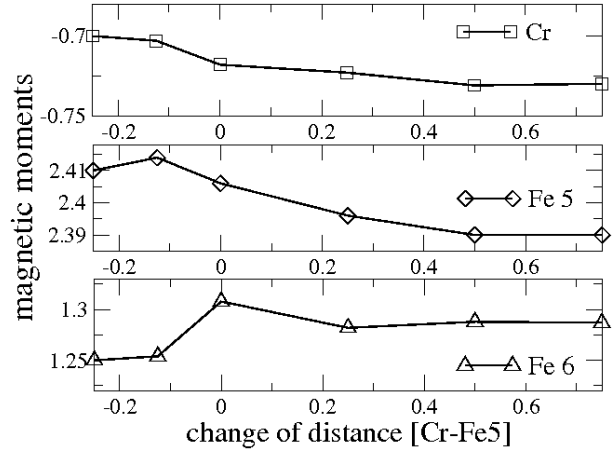


Fig. 3. Local magnetic moments (in μ_B) of the atoms in Fe5-Cr-Fe6 triad versus the displacement $\Delta = [\text{Fe5-Cr}] - [\text{Fe5-Cr}]^0$ of Cr along the (100) axis. Here $[\text{Fe5-Cr}]^0$ is the equilibrium distance between Fe6 and Cr.

d -electronic states [15,16,17,18]. In our work, the Coulomb corrections are incorporated within the SIC-variant of the LSDA+ U approximation introduced in Ref. [15]. The results are presented in Fig. 7 for two different values of $U = 2$ eV and $U = 4.5$ eV estimated and employed in Ref. [19,20,21] to account for the electron repulsion of 3d electrons of Fe and Cr. Fig. 7 shows the finite density of states at the Fermi ($E = 0$) level, although larger U leads to a significant suppression of the majority DOS at E_F which suggests a prevailing tendency towards a half-metallic behavior.

In the LSDA-optimized structure, we find that the cell magnetic moment $M_{\text{LSDA}} = 3.84 \mu_B$ is larger than the magnetic moment $M_{\text{LDA}} = 2.88 \mu_B$ in the LDA-optimized cell. Such an enhancement of the magnetic polarization is connected with the substantial distortions $\Delta \mathbf{R}_i$ in the range 0.2 – 0.84 Å and can be considered as a direct evidence of significant magnetoelastic effect. The local Coulomb corrections in the LSDA+ U -calculations result in enhanced spin polarization. Specifically, we obtain $M_{\text{LSDA}} = 4.07 \mu_B$ for $U = 2$ eV, and $M_{\text{LSDA}} = 4.66 \mu_B$ for $U = 4.5$ eV. It is remarkable that in the substitutional alloy Fe-Cr with 12.5% of Cr, the LSDA approach gives the value $3.8 \mu_B$ for the cell magnetic moment which is slightly lower than the magnetic moment for the considered LSDA-relaxed substitutional alloy.

The obtained high spin polarization of the considered interstitial alloys Fe-Cr allows us to suggest these materials as possible candidates for spin polarizers in the spintronic devices. Possible technological applications of artificially generated interstitial alloys would be related to the thin films produced for the needs of modern electronic industry. In such artificial systems, a central question is related to the methods of implantation and positioning of Cr in centers of the edges of cubic bcc lattice of bulk Fe. With the current state of the art, such structural nanoscale manipulation can be confined to the first subsurface layers of ferrite films by the using for instance the methods of opti-

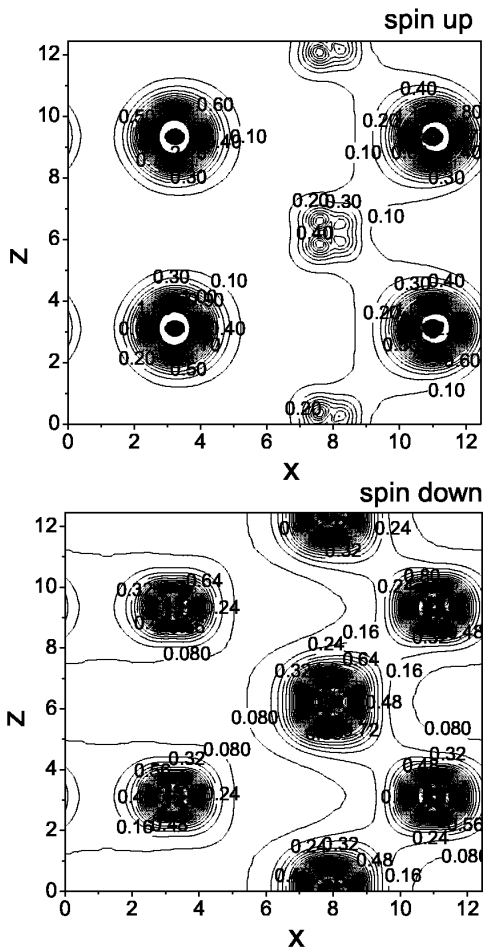


Fig. 4. Contours of electron density maps in the (x, z) -plane ($y/b = 0.25$, x and z given in Å) obtained by integration of electronic states in the energy window E between -3 eV below the Fermi level and the Fermi level. The results obtained by the structural optimization using the LSDA approximation.

cal trapping by lasers [22] or by atomic force microscopy [11]. To estimate the stability of ultra-thin films of iron-chromium alloys which can be also considered as a basis for stainless steels, we have also extended our calculations to the nanoscale two-monolayers-thick iron films containing one interstitial Cr atom per each 20-25 subsurface Fe atoms [12]. For such type of films, we have performed the calculations of the surface formation energy and of the electronic work functions, which were also compared to the corresponding quantities in the films of standard substitutional Fe-Cr alloys. In the interstitial Fe-Cr films, we find that the energy of the surface formation is about 1.69eV and the electronic work function amounts to 1eV, whereas for the substitutional Fe-Cr films we obtain 2.56eV for the surface energy and 0.57eV for the work function. These results allow us to expect high stability and durability of films generated on the basis of nanoscale-manipulated interstitial Fe-Cr alloys, as compared to the iron films with substitutional Cr impurities.

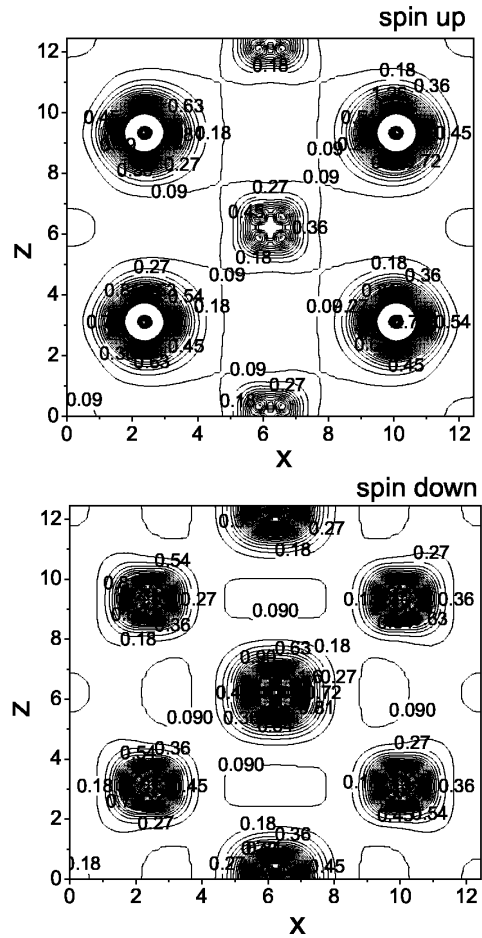


Fig. 5. Contours of electron density maps in the (x, z) -plane ($y/b = 0.25$, x and z given in Å) calculated by integration of electron states in the energy window E between -3 eV below the Fermi level and the Fermi level. The LSDA results obtained in the initially LDA-relaxed structure.

3 Migration paths of N in interstitial alloys $\text{Fe}_\alpha\text{-Cr}$

A central question related to the stability of the considered interstitial alloys is how various atomic impurities can modify the electronic properties. In the structurally relaxed alloys, the chains of atomic Fe-groups are separated by 4Å-wide atomic empty channels, which are expected to contain pathways for light impurity atoms like H, N or Li. To explore a possibility of the migration of the impurities, we consider possible migration paths of a single nitrogen atom in the vicinity of the atomic Fe-chains in the interstitial $\text{Fe}_\alpha\text{-Cr}$.

In the studies of the migration paths of N impurities, we employed the nudged-elastic-band (NEB) method implemented in the Quantum-Espresso (QE) Package for the DFT calculations with the use of plane-wave basis sets and pseudopotentials [23,24]. In these calculations, for the atomic cores of Fe and Cr we employ the Perdew-Burke-Ernzerhof (PBE) norm-conserving pseudopotentials [25].

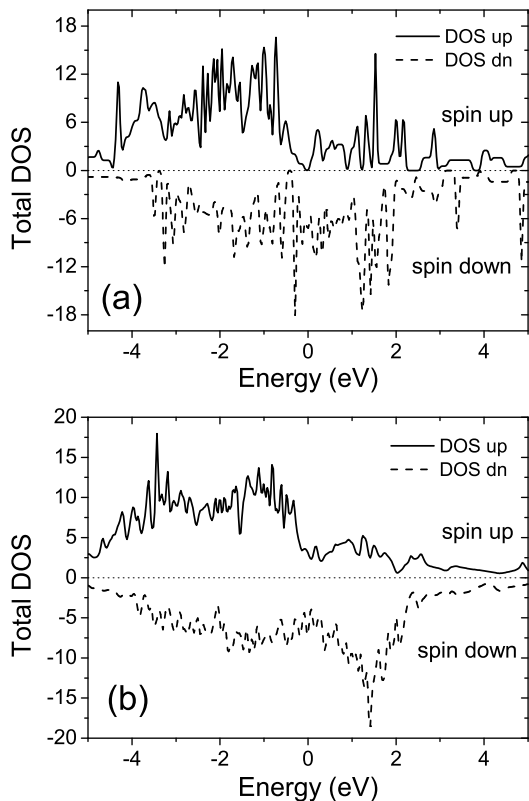


Fig. 6. Total density of states (in eV^{-1}) for structures optimized using (a) LDA approach and (b) spin-polarized LSDA approximation. The Fermi level corresponds to $E = 0$.

For each stage of the nitrogen transport, the NEB method involves a relaxation of the atomic positions and of the distances between the different atoms in the supercell until the forces acting on the atoms reach their minima. In these calculations, we use the plane-wave cutoff 680 eV and the energy cutoff for charge and potential given by 1360 eV. In the NEB-approach, the relaxation of the atomic positions along the nitrogen migration path is performed by the minimization of the total energy of each intermediate configuration (image). These images correspond to different positions of N on the migration path and they are produced by the optimization of a specially generated object functional (action) with the consequent minimization of the spring forces perpendicular to the path. In our calculations, the convergence criteria for the norm of the force orthogonal to the path is achieved at the values below $0.05\text{eV}/\text{\AA}$. As the initial atomic configuration, the supercell Fe-Cr relaxed by the full-potential LSDA-approach [13] has been considered.

Recent studies of the migration paths of single hydrogen atoms by the pseudopotential NEB method demonstrate a good agreement of the obtained transport mechanisms and energy barriers with the experimental measurements [26]. Similarly to Ref. [26], in the present studies, each NEB-generated configuration has been modified by the introduction of the N atom and the obtained in this

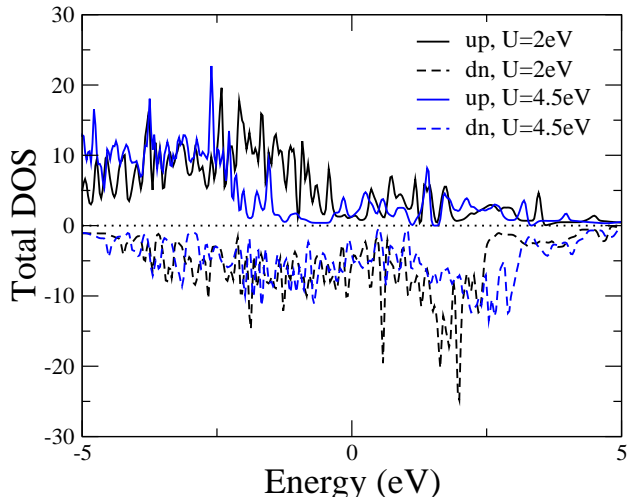


Fig. 7. Total densities of states (in eV^{-1}) for the LSDA-optimized structure calculated by the LSDA+ U method with the local Coulomb corrections for the 3d-orbitals of Fe and Cr $U = 2$ eV (black curves) and 4 eV (blue curves). The Fermi level corresponds to $E = 0$.

way extended supercell has been fully structurally optimized.

To study the migration of N, we consider two different migration paths across the atomic Fe-chains in the Fe-Cr supercell. The first path (path (a)) describes the migration of N from the initial position inside the cell ($z/c = 0.5$) near the chain (1) across the channel to the chain (2) schematically presented in Fig. 8(a). In distinction to the path (a), the second path (b) reflects path2 in Fig. 2(c) and contains additional migration step of N from the supercell boundary ($z \approx 0$) along the c -direction inside the supercell, with the further relocation through the channel to the atomic Fe-chain (2) indicated in Fig. 8(b).

Fig. 9 shows the profiles of the total energy calculated along the N migration paths (a) and (b). The path (a) is characterized by the high energy barriers about 0.8 eV in the path coordinate range ($0 \leq r/R_N \leq 0.4$) and ($0.8 \leq r/R_N \leq 1$) which corresponds to the migration of N within the two Fe-chains (1) and (2). Here R_N denotes the maximal length of the N path in the supercell which reaches about 1 nm for the path (a). The interchain motion inside the channel is signified by a low energy barrier about 0.2 eV ($0.4 \leq r/R_N \leq 0.7$ in Fig. 9(a)).

In contrast to this, the energy profile for the migration path (b) (Fig. 9(b)) contains a plateau-like region at $0.1 \leq r/R_N \leq 0.4$. This migration step indicates the intracell replacement of N near the Fe-chain (1) along the [001]-direction demonstrated in Fig. 4, with a further relocation between the atomic chains across the atomic-empty channel with a low energy barrier about 0.2 eV.

As a conclusion, we can note that the possible migration paths of the light atoms in the considered interstitial Fe-Cr alloys contain a combination of the motion (i) within the atomic-empty channels and (ii) along the c -direction along to the Fe-contained atomic chains.

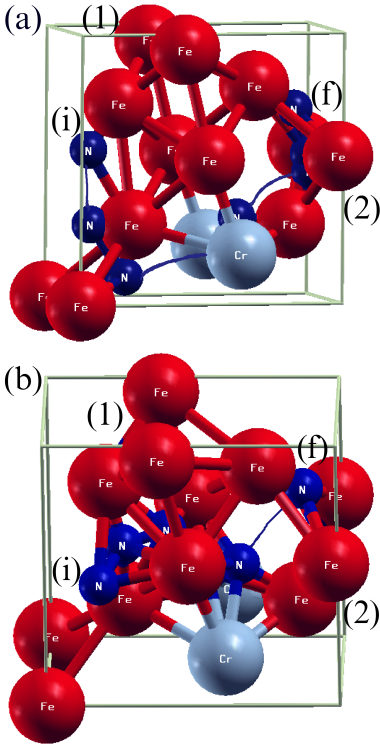


Fig. 8. Two different migration paths of nitrogen through the channel of the optimized crystal cell of Fe-Cr. The top picture (a) represents the interchain migration of N inside the cell with the coordinate z/c near 0.5. The bottom picture (b) corresponds to the migration of N from the c boundary ($z = 0$) along the z direction with the further migration between two neighbouring Fe-chains. The symbols (1) and (2) denote the different atomic chains; (i) and (f) correspond to the initial and final positions of nitrogen in the migration paths.

The question which arises due to the inclusion of N in the magnetic Fe-Cr alloy is how the N impurities modify the magnetic properties of the system. In the work I. Mazin[27], a comparison of the degrees of spin-polarization (DSP) calculated for Fe in the static limit through the density of electronic states, via the current densities and the ballistic limit is presented. It is shown that all the definitions of the DSP give very similar behavior for due to strong hybridization of the sp and d states at the Fermi level. Thus we expect that in the considered Fe alloy with relatively low concentration of Cr it is sufficient to study the static spin polarization in order to capture the main properties of the alloy. Fig. 10 presents the change of the cell and atomic magnetic moments at the migration of N along the path (a) and path (b). Although the nitrogen is initially nonmagnetic in the bulk, it becomes weakly magnetic inside the Cr-Fe alloy with a small magnetic moment $-0.04 \mu_B$ induced by the magnetism of the surrounding. It is noteworthy that the cell magnetic moment is increased to $4 \mu_B$ as N approaches Cr and the distance $[N-Cr]$ becomes about 1.95 \AA . Such an enhancement of M_{tot} is explained by the strong atomic distortions

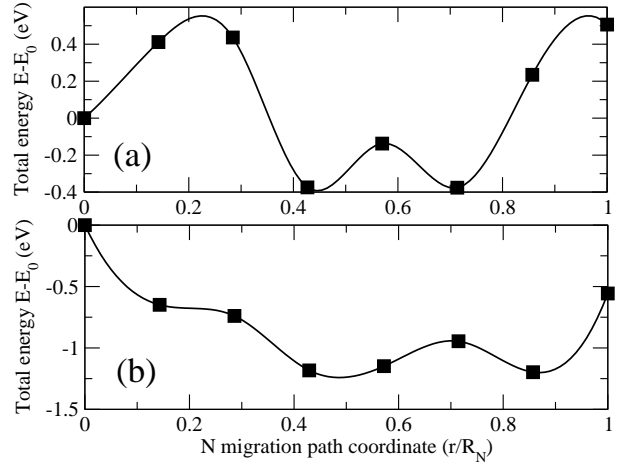


Fig. 9. Total energy profiles of the system along the migration paths of N. Here E_0 denotes the energy of the system in the initial position of N and R_N is the N coordinate in the final position of the path.

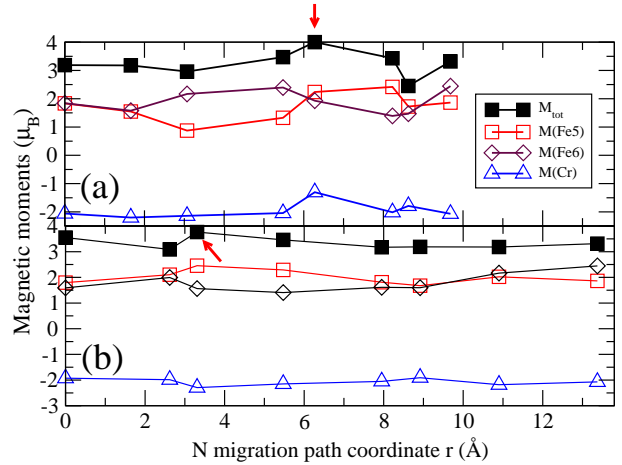


Fig. 10. Cell (M_{tot}) and atomic magnetic moments (in μ_B) along the migration paths of N. The red arrows identify the maximal cell magnetic moments approached upon the minimization of the distance $[N-Cr]$ along the N migration paths.

in the range between 0.04 \AA (Fe7) up to 0.2 \AA (Fe3) caused by the replacement of N and by the consequent magnetoelectric effect. In Fig. 10, the increase of the distance from N to Cr suppresses the magnetic moment of N and decreases the cell magnetic polarization to the typical values about $3.5 - 3.8 \mu_B$ obtained in LSDA-calculations for the artificial Fe-Cr alloys. The obtained drastic change of the magnetic polarization clearly demonstrates a crucial importance of the location of nonmagnetic impurities like N for the electronic properties of alloy. As follows from our findings, a control of the location of N, for example by external electric field, can lead to externally tuned changes of the magnetic polarization, a feature which is of central importance for possible spintronic devices based on the artificial Fe-Cr alloys.

4 Conclusion

We have performed the DFT studies of the bulk ferrite with 12.5%-concentration of monoatomic interstitial Cr periodically located at the edges of the bcc Fe_α cell. We have shown that the full atomic relaxation of the obtained interstitial Fe-Cr stabilizes a new chain-like low-symmetry structure. In this structure, the monoatomic Cr at the edges of ferrite bcc cells leads to the local atomic distortions and results in the formation of parallel chains of Fe_6 -octahedra, which are connected by the interchain Fe-Cr bonds. The significant energy gain caused by such a structural relaxation approaches 6.17 eV which makes this type of interstitial alloy highly stable and energetically favorable with the negative formation energy approaching -1.15 eV. The novel electronic state of the system can be characterized as metallic, where the metallic properties is the result of strong Fe-Cr hybridization of the structurally relaxed alloy. In the investigations of the magnetic state of the generated relaxed structures, we have obtained a local antiferromagnetic order in the close proximity of Cr atoms, whereas the more distant Fe atoms are coupled ferromagnetically. We also find that the nonmagnetic impurities like nitrogen can substantially modify the magnetic properties of the interstitial alloy which can be considered as an additional manifestation of the strong magnetoelastic effect in this type of alloys. We propose to consider the generated interstitial alloys as perspective candidates for fabrication of novel highly durable stainless steels and for possible applications in spintronic and multifunctional devices.

5 Acknowledgements

This work has been partially supported through the project "Models of quantum statistical description of catalytic processes on metallic substrates" of the Ministry of Education and Sciences of Ukraine and the grant 0108U002091 of the National Academy of Science of Ukraine. A grant of computer time from the Ukrainian Academic Grid is acknowledged.

References

1. D. Peckner and I.M. Bernstein. *Handbook on Stainless Steels*, McGraw-Hill Book Co., New York, 1977.
2. A. Mai, V.A.C. Haanappel, S. Uhlenbruck, F. Tietz, and D. Stöver, *Solid State Ionics*, **176**, 1341 (2005).
3. H. Yokokawa, H. Tu, B. Iwanschitz, and A. Mai, *J. Power Sources*, **182**, 400 (2008).
4. R.H. Victora and L.M. Falicov, *Phys.Rev.B* **31**, 7335 (1985).
5. A.T. Paxton and M.W.Finnis, *Phys.Rev.B* **77**, 024428 (2008).
6. C. Paduani and J.C. Krause, *Braz. Journ. of Physics*, **36**, 1262 (2006).
7. A. Davies, J.A. Stroschio, D.T. Pierce, and R.J. Celotta, *Phys.Rev.Lett*, **76** 4175 (1996).
8. T.P.C. Klaver, P. Olsson, and M.W. Finnis, *Phys.Rev.B* **76**, 214110 (2007).
9. P. Olsson, C. Domain, and J. Wallenius, *Phys.Rev.B* **75**, 014110 (2007).
10. Z.A.Duriagina and M.I.Pashechko, *Metal Science and Treatment of Metals*, **4**, 34 (2000).
11. Y. Sugimoto *et al.*, *Science* **322**, 413 (2008).
12. N. Pavlenko, unpublished.
13. P. Blaha, K. Schwarz, G.K.H. Madsen, D. Kvasnicka, and J. Luitz, *WIEN2K, An Augmented Plane Wave + Local Orbitals Program for Calculating Crystal Properties*, ISBN 3-9501031-1-2 (TU Wien, Austria, 2001).
14. J.-H. Park *et al.*, *Nature* **392**, 794 (1998).
15. V.I. Anisimov, I.V. Solovyov, M.A. Korotin, M.T. Czyzyk, and G.A. Sawatzky, *Phys.Rev. B* **48**, 16929 (1993).
16. M.T. Czyzyk and G.A. Sawatzky, *Phys.Rev. B* **49**, 14211 (1994).
17. N. Pavlenko, *Phys. Rev. B* **80** 075105 (2009).
18. N. Pavlenko, I. Elfimov, T. Kopp, and G.A. Sawatzky, *Phys. Rev. B* **75**, 140512(R) (2007).
19. T. Bandyopadhyay and D.D. Sarma, *Phys.Rev. B* **39**, 3517 (1989).
20. Ze Zhang and S. Satpathy, *Phys.Rev. B* **44**, 13319 (1991).
21. M.A. Korotin, V.I. Anisimov, D.I. Khomskii, and G.A. Sawatzky, *Phys.Rev.Lett.* **80**, 4305 (1998).
22. A. Ashkin. *Optical trapping and manipulation of neutral particles using lasers*, World Scientific Pub., Singapore, 2006.
23. P. Giannozzi *et al.*, *J. Phys. Cond. Matter* **21**, 395502(2009).
24. H. Jonsson, G. Mills, and K.W. Jacobsen, *Nudged Elastic Band Method for Finding Minimum Energy Paths of Transitions in Classical and Quantum Dynamics in Condensed Phase Simulations in Classical and Quantum Dynamics in Condensed Phase Simulations*, ed. by B.J. Berne, G. Ciccoti, and D.F. Coker (Singapore: World Scientific, 1998).
25. J.P. Perdew, S. Burke, and M. Ernzerhof, *Phys. Rev. Lett.* **77**, 3865(1996).
26. N. Pavlenko, A. Pietraszko, A. Pawlowski, M. Polomska, I.V.Stasyuk, and B. Hilczer, *Phys. Rev. B* **84**, 064303 (2011).
27. I. Mazin, *Phys. Rev. Lett.* **83**, 1427(1999).